**RESEARCH ARTICLE**

# Performance of river sediments after flocculation-pressure filter membrane-vacuum preloading

Linzhu Sun[1] · Yunyun Zheng[1] · Xiaoniu Yu[1,2]

## Abstract

The main problem in the reduction of river bottom sediments is to solve the dewatering of the sludge. The commonly used natural air drying method requires a large amount of time and economic cost. In this paper, different treatments were developed for the needs of the project, and related tests were carried out on the reduction of the sludge. Firstly, two or more flocculants were compounded according to the nature of the sludge. The 6 different treatments were determined according to the sedimentation and the turbidity value of the supernatant. Secondly, the dewatering test was carried out on river sediments after flocculation-vacuum preloading. The dewatering effect of different flocculants, water quality, dissipation of pore water pressure, vane shear strength, compression coefficient, and coefficient of consolidation have been analyzed after flocculation-vacuum preloading. The polysilicate aluminium ferric (PSAF) can greatly increase the dewatering efficiency of the filter press membrane, and the final dewatering amount could reach 310 g. The effect of purifying water quality was PSAF>PAM (polyacrylamide, PAM-1(18 million): PAM-2(23 million) = 3:7)>PAC (polyaluminium chloride). The PSAF and PAC could increase the pH of the water during the vacuum preloading test. The PAM has the best the vane shear strength. Lime could improve the vacuum preloading and the vane shear strength when it was added to other flocculants. The incorporation of PSAF could accelerate the dissipation and increase the final dissipation value of pores water pressure. Compared with PAM+PAC+lime, PAM+lime, PAM+PSAF+lime, PAM+PSAF, and PAM+PAC, the overall effect and price of the PAM is optimal.

**Keywords** River bottom sediments · Flocculation effect · Vacuum preloading · Vane shear strength · Compression coefficient

## Introduction

The pressure of the environment and society has been increased in the face of river sediments because of the rapid development of industrial production and cities. Many countries around the world have paid more and more attention to treatment of river sediments (Fang et al. 2019a, b; Akcay et al. 2003; Pejman et al. 2015; Teatini et al. 2011; Jankowski et al.

2017; Liu et al. 2019; Liu and Cai 2019; Trojanowska and Świetlik 2019). Treatment methods of river sediments are different depending on the national conditions of different countries. In early 1989, the US Environmental Protection Agency has proposed the rules for the treatment and utilization of the sediments from domestic sewage plants: land application, landfill, site surface treatment, and incineration. The use and incineration are development direction of the sediments disposal in the perspective of sustainable development.

In recent years, the dewatering sediments have been widely used as a fertilizer in agriculture and street greening in the Japan. At the same time, the mainstream treatment method of the sediments is to use incineration ash and slag as building materials for the purpose of reduction and stabilization. The treatment process of the sediments is as follows: concentration→ dewatering →incineration, concentration→ digestion→ dewatering→ incineration, and concentration→ digestion→ dehydration. Up to 61% of the total sediments are treated by above three methods. The Japanese sediments are usually burned, but the cost is expensive. Reducing the drying

---

Responsible editor: Angeles Blanco

✉ Xiaoniu Yu
  xnyu09@163.com

[1] College of Civil Engineering and Architecture, Wenzhou University, Wenzhou 325035, China

[2] School of Environment, Tsinghua University, Beijing 100084, China

time and speeding up the dewatering rate of the sediments are very important to solve dredging problem in the whole river regulation.

The most obvious characteristics of the river sediments are dirty and stinky, and it will also cause siltation of the river, causing the river bed to rise. The shipping and water storage capacity will be weakened. The traditional treatment method of the sediments is to do fertilizer or air storage and landfill. However, air storage takes up a lot of space and will cause secondary pollution. The river sediments are scientifically processed which can be well utilized in different fields. (1) The river sediments are used as agricultural fertilizer and fuel (Emelyanov and Kravtsov 2007; Xia et al. 2012). (2) The river sediments are used for brick making after incineration (Liu et al. 2018; Lafhaj et al. 2008; Samara et al. 2009). (3) The river sediments are used as filling material and road construction material by adding a certain amount of curing agent.

There are many rivers in Zhejiang Province, China, and there are more than 60,000 km of various rivers, including more than 40,000 km of plain rivers. At present, the total river siltation in the province is nearly 2 billion $m^3$, of which the Hangjiahu plain has siltation of 394 million $m^3$ and the Qiantang river has nearly 500 million $m^3$. The Minjiang river has more than 800 million $m^3$. These rivers continue to silt at a rate of 100 million $m^3$ per year. The main problem in the reduction of river bottom sediments is to solve the dewatering of the sediments. The commonly used natural air drying method requires a large amount of time and economic cost. The 6 different treatments were selected for flocculation of river sediments through screening in the paper. Compared to natural air drying method, the river sediments were reduced by flocculation-pressure filter membrane-vacuum preloading in a short time. Water quality and performance parameter of river sediments were then analyzed after flocculation-vacuum preloading test.

## Experiment and methods

The sediments were taken from the river bottom section of the Hualong bridge in Wenzhou, China. Particle size distribution curve, physical properties, and minerals content of river sediments were shown in Tables S1 and S2. The relative moisture content of the sample was $60.6 \pm 0.2\%$ which is lower than dredged fill, and the sample was flowing state (Zhu et al. 2013; Wang et al. 2019) (see Supplementary information). Polyacrylamide, polyaluminium chloride, chlorinated high iron, polymeric aluminum silicate iron, etc. were used in this study. Among them, polyacrylamide adopts ionic type as anionic polyacrylamide, and the molecular weight was 18 million and 23 million, regards as PAM-1 and PAM-2, respectively. Polyaluminium chloride (PAC, solid, $Al_2O_3$ content = 28%, basicity = 40–90%) was used and produced by Hefei Zicheng Environmental Protection Technology Co., Ltd.. Polysilicate

aluminium ferric (PSAF, solid, $SiO_2$ content = 0.8–1.5%, $Al_2O_3$ content ≥ 24–28%, Fe content ≤ 1.5–3.5%, basicity = 40–90%) was made by Henan Taiyuan Environmental Protection Technology Co., Ltd. The pH of the adapted water is between 6 and 9. Lime was slaked lime, produced by Liyang Zhenxin Chemical Co., Ltd. (Table S4). These chemicals and dosages were selected and mention the details of this selection can be found in "Supplementary information" according to flocculation effect and price. A portable turbidity meter was purchased from the American HACH Company (HACH 2100Q). All experiments were repeated three times.

## Flocculation-pressure filter membrane test

The 6 groups of flocculants were determined according to the sedimentation and the turbidity value of the supernatant, as shown Tables S5-S8 and Figures S2-S3. The test equipment included a 500-mL beaker, a graduated cylinder, a timer, an electronic balance, a blender, and so on. The 400 mL of the sediments was weighed according to the experimental design. After calculating the mass of the river sediments, PAM+PAC+lime (A), PAM+lime (B), PAM+PSAF+lime (C), PAM+PSAF (D), PAM (E), and PAM+PAC (F) were weighed and added to the sediments, and stirred evenly (Table 1). Stirring time was between 4 and 5 min. After being placed for 2–3 h, it was loaded into a self-made hydraulic pressure filter device. The sediments thickness was controlled at 40 cm and the hydraulic pressure was maintained at 800 kPa. Filter press time, temperature, and relative humidity were 300 min, $25 \pm 2$ °C, and 70–80%. The 7 sets of experiments were designed according to above data.

In tests, the dewatering amount of the sediments was read once every 5 min. After 100 min, it was read once every 10 min, and the pressure filtration time lasted for 300 min. The dewatering amount of the sediments was recorded with the change of the filtration.

The flocculation-vacuum preloading method was used in these tests (Kjellman 1952; Chai and Rondonuwu 2015; Sun et al. 2018; Wang et al. 2019a). The purpose of these tests was

Table 1  Combination methods and dosage of flocculants

| No. | PAM (PAM-1: PAM-2 = 3:7) | PAC | PSAF | Lime |
|-----|--------------------------|---------|------|--------|
| A | 0.08% | 0.0133% | – | 0.0625% |
| B | 0.08% | – | – | 0.0625% |
| C | 0.08% | – | 0.05% | 0.0625% |
| D | 0.08% | – | 0.05% | – |
| E | 0.08% | – | – | – |
| F | 0.08% | 0.0133% | – | – |

Note: A = PAM+PAC+lime; B=PAM+lime; C = PAM+PSAF+lime; D = PAM+PSAF; E = PAM; F=PAM+PAC

to study the effect of different flocculants on the vacuum consolidation of the river sediments. The vacuum preloading of the soil samples was taken from the Hualong Bridge in Wenzhou, and the initial moisture content was about 60%. The test equipment included a model bucket with a diameter of 30 cm and a height of 40 cm, a vacuum pump, a drainage plate, a water vapor separation bottle, a vacuum gauge, a vacuum tube, a geotextile, and a geotextile cloth. In the experiment, the river sediments without flocculants were set as the control group, and a total of 7 model buckets were set. The 6 flocculants were shown in Table 1.

The detection error caused by the deformation could be reduced when the position of the test equipment such as the drainage board, vacuum degree probe, and pore pressure sensor was well fixed. Secondly, the vacuum film was laid on the inner wall of the model barrel, and the flocculation soil was poured into. The frame was slowly placed in the center of the model bucket. After completion, a layer of 150 g/m$^2$ geotextile and non-woven geotextile was laid on the surface to protect the vacuum film used for sealing. The non-woven geotextile was not less than 250 g/m$^2$. Then, a layer of polyvinyl chloride vacuum film was laid on the surface of the geotextile to make the model barrel a sealing system. Finally, the hose connected to the drainage board in the model barrel was connected with the water vapor separation bottle. The quality of the water vapor separation bottle was used to determine the displacement according to the record. The other end of the water vapor separation bottle was connected to the vacuum pump, and a vacuum was applied to generate a negative pressure inside and outside the vacuum membrane. Under the action of the negative pressure, the water and air in the soil were quickly discharged through the drainage plate, so that the soil was consolidated rapidly. A schematic diagram of the test model device was shown in Fig. 1. The vacuum

pump was started in the vacuum preloading test when the above steps were completed. During the test, the vacuum degree of the vacuum pump was maintained at about 800 kPa.

The displacement of each test in real time was recorded. The vacuum degree in the drainage board at depth of 0 cm, 20 cm, and 40 cm from the surface of the soil was recorded in real time. The pore water pressure was recorded at depth of 20 cm and 40 cm. (1) The water content and the shear strength of the cross plate at depth of 0 cm, 20 cm, and 40 cm were measured from the surface of the soil after the vacuum preloading test. (2) Consolidation effect of the soil was tested at depth of 0 cm and 40 cm from the surface of the soil after the vacuum preloading test. (3) The turbidity and pH were measured after the vacuum preloading test. (4) Each group of the flocculation soil was taken for the determination of liquid-plastic limit and analysis of particles gradation.

## Results and discussion

### Flocculation-pressure filter membrane test

The relationship between dewatering amount and time was obtained according to the change of dewatering amount of the river sediments in each group, as shown in Fig. 2. The effect of different flocculants on the dewatering performance of the river sediments is different under the same test conditions. It can be seen from Fig. 2 that the dewatering amount of PAM+PSAF+lime and PAM+PSAF is between 2 and 3 times more than that of the other groups after flocculation.

The PAM+PAC+lime (A) and PAM+PAC (F), PAM+lime (B) and PAM (E), PAM+PSAF+lime (C), and PAM+PSAF (D) discussed the effect of lime incorporation on the flocculation-pressure filter membrane. In PAM+PAC+lime

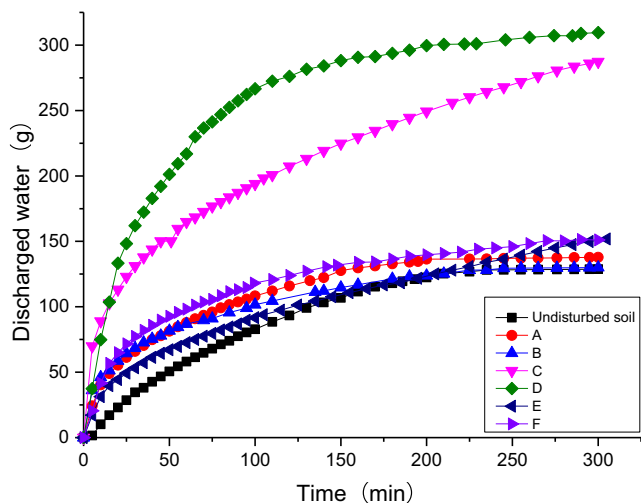**Fig. 1** Schematic diagram of the vacuum preloading test
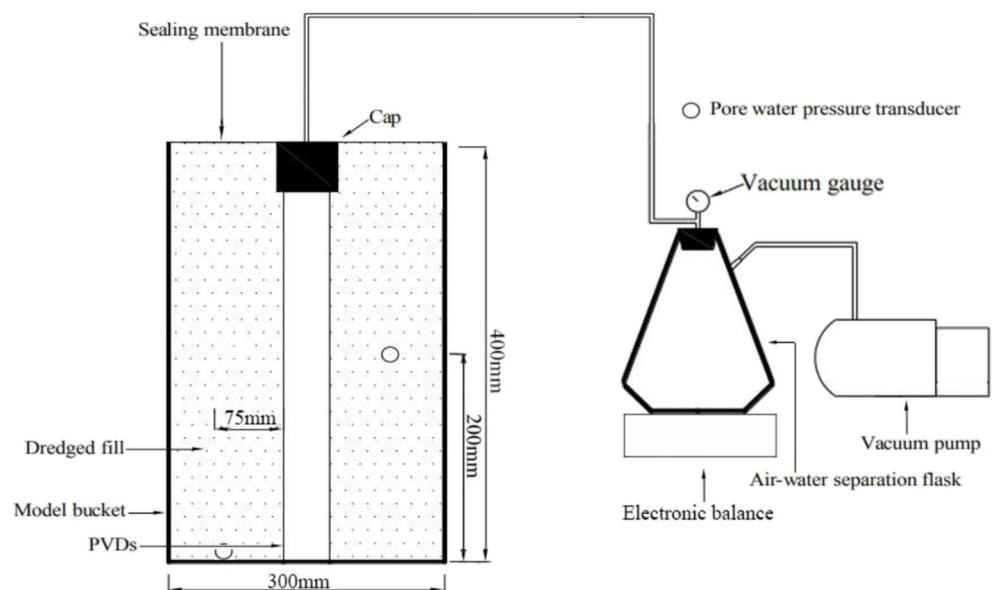
**Fig. 2** Dewatering amount and time curve of flocculation-pressure filter diaphragm test (PAM+PAC+lime (A), PAM+lime (B), PAM+PSAF+lime (C), PAM+PSAF (D), PAM (E), and PAM+PAC (F))



**Fig. 3** Relationship curve of $w_0$-h

and PAM+PAC, the final displacement of the PAM+PAC is 151 g, and that of the PAM+PAC+lime is 137.8 g. The dewatering speed of the two groups decreases with time. In PAM+lime and PAM, the final displacement of the PAM is 152 g, and the PAM+lime is 130 g. The overall growth trend of the final displacement for PAM+PAC+lime, PAM+PAC, PAM+lime, and PAM is similar, which exceeds the control group by 129 g. In PAM+PSAF+lime and PAM+PSAF, the final displacement of the PAM+PSAF is 310 g, and the PAM+PSAF+lime is 287 g. In the PAM+PSAF, the growth rate of the sediments dewatering is faster than that of other groups in the first 100 min. The displacement in 100 min exceeds the maximum of other groups. At 300 min, it is far more than other groups.

It is obvious that the incorporation of lime affects the effect of pressure filtration dewatering, so that the displacement is reduced by about 15–20 g. The incorporation of PAC can slightly increase the speed of drainage and the final displacement. The PSAF can greatly increase the dewatering efficiency of the filter press membrane, and the final dewatering amount can reach up to 310 g.

## Determination of liquid limit and plasticity of soil particles

The liquid limit and plastic limit of each group are calculated according to $w_0$-h relationship curve, as shown in Table 4. The $w_0$-h relationship curve of the soil samples is shown in Fig. 3.

According to the Geotechnical Test Standard, the water content is the liquid limit of the soil when the sinking depth is 17 mm. When the sinking depth is 2 mm, the water content is the plastic limit of the soil in the relationship curve of $w_0$-h. All values are expressed as a percentage, accurate to 0.1%. At
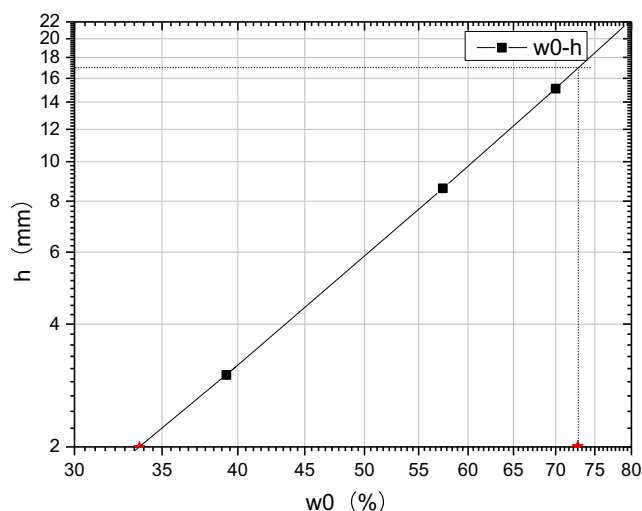
the same time, the plasticity and liquidity index are calculated according to Eq. 1 (Huang et al. 2019):

$$I_P = w_L - w_P, I_L = \frac{w_0 - w_P}{I_P} \tag{1}$$

where $I_p$ represents plasticity index; $I_L$ is the liquidity index, calculated to 0.01; $w_L$ represents liquid limit (%); $w_p$ is the plastic limit (%); and $w_0$ is the natural moisture content (%).

It can be seen from Table 2 that the addition of the flocculants has a great influence on the liquid limit of the soil. The liquid limit of all soils is increased by 13.7–24.5%. However, the addition of flocculants has little effect on the plastic limit of the soil. In PAM+PAC+lime and PAM+PAC, the flocculants keep the plastic limit substantially constant or slightly increased, and the addition of lime greatly increases the plastic limit of the soil, because the alkaline environment can be created by addition of the lime to the PAM+PAC. The lime can increase plasticity index of the soil (17.1–45%) in the PAM+PAC+lime. The result indicates that the content of bound water in the soil is increasing, which is conducive to the later drainage consolidation.

In PAM+lime and PAM, the flocculants slightly reduce the plastic limit of the soil. The effect of lime on the plastic limit was not obvious, and the reduction range was about 7%. Compared to PAM+PSAF+lime and PAM+PSAF, the liquid limit and plasticity index of the soil were increased; however, the plastic limit was decreased. The decrease of the plastic limit indicates that the flocculants have a certain influence on the particles size.

The percentage of the mass of the soil is smaller than a certain particle diameter to the total mass of the sample is the ordinate. The particles size is the abscissa. The particles size distribution curves are plotted on the single logarithmic coordinate according to Table 3. The curves result is shown in Fig. 4. Figure 4 shows the particles size distribution curves of the control group and PAM+PAC+lime (A), PAM+lime (B), PAM+PSAF+lime (C), PAM+PSAF (D), PAM (E), and

**Table 2** Results of liquid and plastic limits of each group

| No. | Liquid limit (%) | Plastic limit (%) | Plasticity index | No. | Liquid limit (%) | Plastic limit (%) | Plasticity index |
| --- | --- | --- | --- | --- | --- | --- | --- |
| Blank | 72.78 | 34 | 38.98 | D | 86.95 | 32.27 | 54.68 |
| A | 82.76 | 37.11 | 45.65 | E | 90.62 | 31.78 | 58.84 |
| B | 83.98 | 31.5 | 52.48 | F | 90.15 | 33.63 | 56.52 |
| C | 87.19 | 31.92 | 55.28 | | | | |

Note: A = PAM+PAC+lime; B = PAM+lime; C = PAM+PSAF+lime; D = PAM+PSAF; E = PAM; F = PAM+PAC

PAM+PAC (F) groups. It can be found that the flocculants make the curves gentler, and the particles size difference of the test soil is more disparate. The particles distribution is uneven and the gradation is good.

It can be seen from Fig. 4 that, especially in the PAM+ PAC+lime, PAM+PAC, PAM+lime, and PAM, the incorporation of lime continues to increase the particles size of the soil particles. At the same time, the coefficient of nonuniformity $Cu$ and the coefficient of curvature $Cc$ of each group are calculated and obtained in Table 3 (Zhu et al. 2011).

It can be seen from Table 3 that PAM+PAC+lime (A), PAM+ lime (B), PAM+PSAF+lime (C), PAM+PSAF (D), and PAM (E) can reduce the $Cu$ and the distribution range of the soil particles, but the gradation is still continuous and good from the coefficient of nonuniformity. The PAM+PAC increases the $Cu$ of the soil and expands the distribution range of the particles size, making the soil particles more uneven, but the gradation is better. The $Cc$ of PAM+PAC+lime, PAM+lime, PAM+PSAF+lime, and PAM+ PSAF are not different in the coefficient of curvature. It also shows that the gradation distribution of PAM+PAC+lime, PAM+lime, PAM+PSAF+lime, and PAM+PSAF is good.

## Dewatering and water quality test after vacuum preloading

In the vacuum preloading process, the mass of the water vapor separation bottle is weighed in real time through the electronic

scale as the displacement of the vacuum preloading test, and the relationship between the displacement and the time is plotted, as shown in Fig. 5. It is found that the drainage volume of the PAM+PSAF is the most, and the water discharge rate is also the fastest in the first day. The control group without flocculants is the lowest in the vacuum preloading, and the effect is the worst. The water output of the PAM+PSAF is 187% of the control group at the same time. The PAM+ PAC+lime and PAM+PAC have poor drainage. The initial stage is slow, but the overall effect is still better than the control group. The water output of PAM+PAC+lime and PAM+ PAC is 172% and 161% of the control group, respectively. It can be seen from Fig. 5 that the addition of lime reduces the drainage rate and the final displacement. This may be due to the reaction of lime with silica in the soil, and resulting in blocks in the pore channels during vacuum preloading, that can affect the drainage. The drainage rate of the PAM+PAC without lime is faster than the PAM+PAC+lime in the early stage. After 1000 min, the drainage rate of the PAM+PAC+ lime is gradually increased because the PAC produces hydroxide and aluminate in an alkaline environment. Therefore, the effect of reaction of lime with the soil on the pore channels is reduced. Discharged water volume of PAM+PSAF and PAM in the river sediments is similar with dredger fill in PAM and
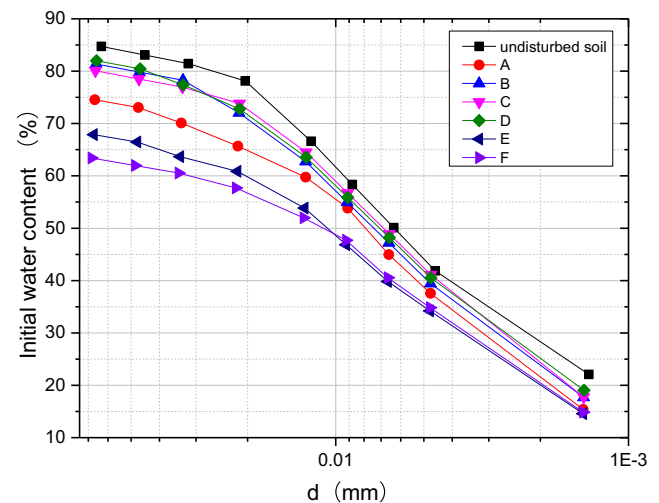
**Table 3** Calculation results of $Cu$ and $Cc$

| No. | $d_{10}$ | $d_{30}$ | $d_{60}$ | $Cu$ | $Cc$ |
| --- | --- | --- | --- | --- | --- |
| Blank | 0.00030649 | 0.002235 | 0.0094 | 30.670 | 1.734 |
| A | 0.00078805 | 0.0031513 | 0.0129 | 16.370 | 0.977 |
| B | 0.00067393 | 0.002812 | 0.0113 | 16.767 | 1.0382 |
| C | 0.00068686 | 0.0026714 | 0.0108 | 15.724 | 0.962 |
| D | 0.00064124 | 0.0026211 | 0.0104 | 16.219 | 1.030 |
| E | 0.00083673 | 0.0036849 | 0.0203 | 24.261 | 0.799 |
| F | 0.00083673 | 0.003563 | 0.0314 | 37.527 | 0.483 |

Note: $d_{10}$, $d_{30}$, and $d_{60}$ are called effective particle size, median diameter, and restricted particle size, respectively. A = PAM+PAC+lime; B = PAM+lime; C = PAM+PSAF+lime; D = PAM+PSAF; E = PAM; F = PAM+PAC



**Fig. 4** Particles size distribution curves of each group (PAM+PAC+lime (A), PAM+lime (B), PAM+PSAF+lime (C), PAM+PSAF (D), PAM (E), and PAM+PAC (F))
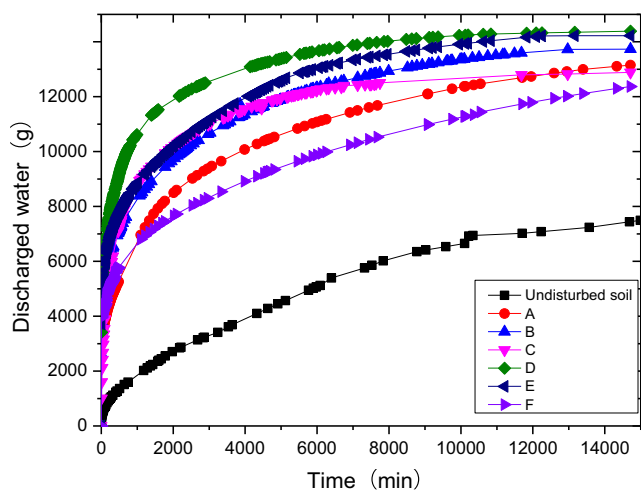
**Fig. 5** Curves of displacement and time in the vacuum preloading (PAM+PAC+lime (A), PAM+lime (B), PAM+PSAF+lime (C), PAM+ PSAF (D), PAM (E), and PAM+PAC (F))

PAM+lime before 6000 min according to literature reported (Wang et al. 2019b).

Figure 6 shows the results of determination of liquid turbidity before and after the vacuum preloading. Before the vacuum preloading, the flocculants of each group are added to make the soil particles form larger flocs, thereby discharging the interstitial water between the soil particles. The turbidity of the water is also obtained and not the same in different flocculants. It can be seen from Fig. 6 that the turbidity after flocculation is the highest in PAM+PAC+lime and PAM+PAC, reaching above 400 NTU. The turbidity of PAM+lime and PAM is between 250 and 290 NTU. The turbidity of PAM+PSAF+lime is the lowest, which is 101.5 NTU. It can be found that the effect of purifying water quality is the PSAF>PAM>PAC.

Figure 7 shows the results of determination of the pH of the liquid before and after the vacuum preloading. The pH of the liquid obtained after flocculation is basically between 6.5 and
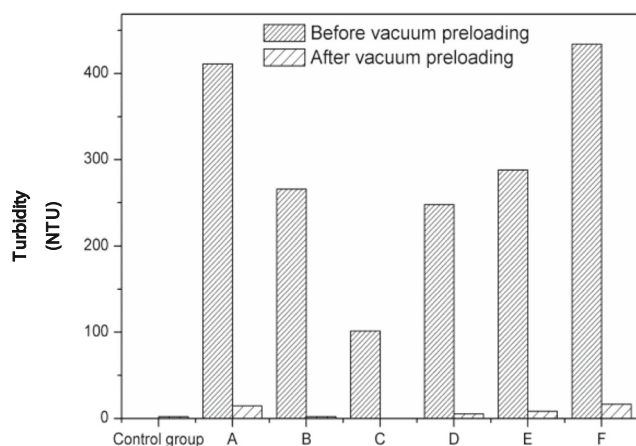


**Fig. 6** Results of turbidity (PAM+PAC+lime (A), PAM+lime (B), PAM+ PSAF+lime (C), PAM+PSAF (D), PAM (E), and PAM+PAC (F))
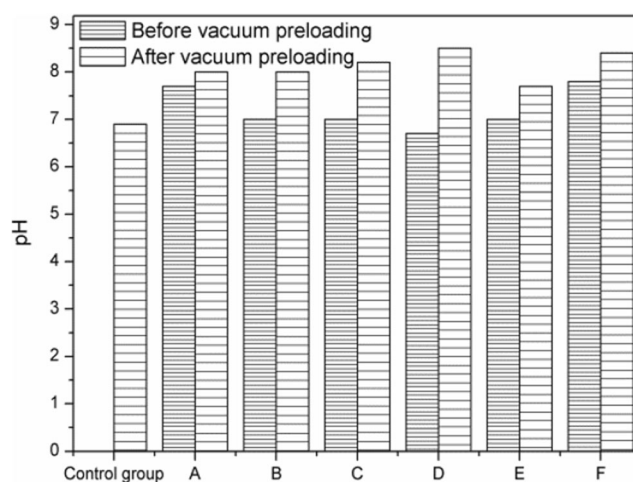


**Fig. 7** Results of pH (PAM+PAC+lime (A), PAM+lime (B), PAM+ PSAF+lime (C), PAM+PSAF (D), PAM (E), and PAM+PAC (F))

8, and the pH is between 7.5 and 8.5 after the vacuum preloading. The PAM+PAC+lime and PAM+PAC are in an alkaline state after the vacuum preloading, and the pH is between 8.0 and 8.5. The pH of PAM+lime and PAM is lower than that of PAM+PAC+lime and PAM+PAC after the vacuum preloading, and the maximum can reach 8. The PAM+ PSAF+lime and PAM+PSAF are in a state of weak alkaline after the vacuum preloading, and the pH is also between 8.0 and 8.5. The PSAF and PAC can increase the pH of the water during the vacuum preloading. The curves of vacuum degree in the drainage plate as a function of time are shown in Figure S4. Data integration of the settlement points in the barrels is shown in Figure S5.

## Vane shear strength

After the vacuum preloading test, the vane shear strength was carried out on the soil at different depths from the surface of the model box using a portable vane shear strength tester. The test results are shown in Fig. 8. Figure 8 shows vane shear strength of the control group, PAM+PAC+lime (A), PAM+ lime (B), PAM+PSAF+lime (C), PAM+PSAF (D), PAM (E), and PAM+PAC (F). The depth of the control group is less than 40 cm after the vacuum preloading. Therefore, the vane shear strength at depth of 0 cm and 30 cm is measured, which is 6.5 kPa and 4 kPa, respectively (Fig. 8a). The vane shear strength of the soil at 0 cm, 20 cm, and 40 cm of depth is measured in PAM+PAC+lime (A), PAM+lime (B), PAM+ PSAF+lime (C), PAM+PSAF (D), PAM (E), and PAM+PAC (F), as shown in Fig. 8b.

As a whole, the vane shear strength decreases with the increase of the depth. The vane shear strength of the PAM is the highest (> 50 kPa), which is greater than other groups and dredged fill in lime (Jin et al. 2019). The strength of the surface layer of PAM+PSAF+lime and PAM+lime is 47 and 45 kPa, respectively. The vane shear strength of PAM+

**Fig. 8** Vane shear strength of the control group, PAM+PAC+lime (A), PAM+lime (B), PAM+ PSAF+lime (C), PAM+PSAF (D), PAM (E), and PAM+PAC (F)



(a)                                                    (b)
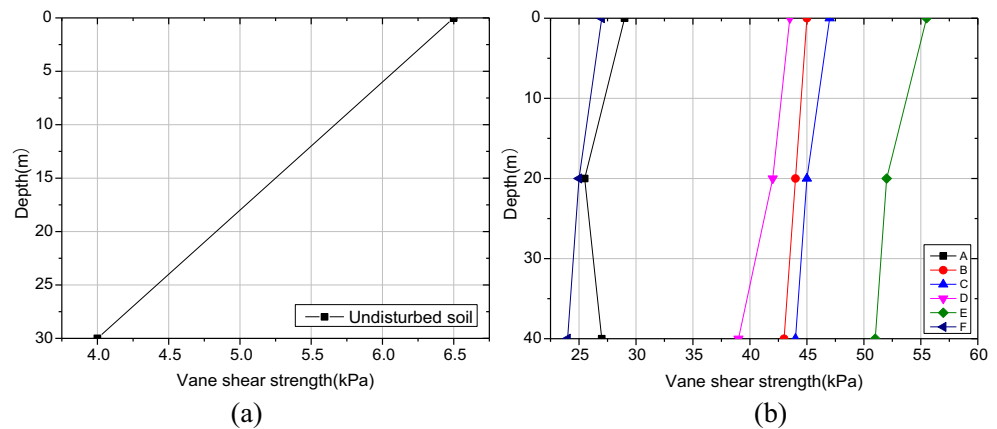
PAC+lime and PAM+PAC is the lowest (< 30 kPa), but this exceeds the control group. Compared to the water content of each group, it can be seen that the lower the water content, the higher the vane shear strength after flocculation. However, the fluctuation of the strength is not large, both of which are about 3 kPa. In the composition of the flocculants, both PAM+PAC+ lime and PAM+PAC are mixed with the polyaluminium chloride. It can be found that the effect of the addition of the polyaluminium chloride on the vane shear strength is not obvious. The PSAF is added into the PAM+ lime and PAM, and the vane shear strength is increased by 10–12 times. The addition of lime does not increase the vane shear strength in the PAM. The addition of lime to the PAC and PSAF can increase the vane shear strength to a certain extent (2–13%). This is mainly due to the flocs formed by the particles during the flocculation process which can be stabilized in the soil skeleton. The stable skeleton structure is advantageous for the vacuum preloading and drainage consolidation, thereby improving the strength. In summary, the PAM has the best effect, followed by the PAM+PSAF+lime. In the case of the two flocculants, the lime can improve the vacuum preloading and vane shear strength. The vane shear strength can be improved after vacuum preloading in different types of flocculants.

## Water content test

The water content of the soil samples at depth of 0 cm, 20 cm, and 40 cm includes the initial water content, the water content after the flocculation, and the water content after the vacuum preloading. It can be seen from Fig. 9 that the initial moisture content of the soil samples is relatively high, reached about 60%, which has good fluidity. After the flocculation test, the water content has been increased to about 65%. Although the water content increased, the soil state is plasticity. After flocculation, the soil particles were wrapped into flocculent precipitates. There is more interstitial water between the soil bodies, which is blocked by the upper flocs during the

sedimentation process, so that a part of the interstitial water cannot be transferred upward, resulting in the increase of the water content. After the vacuum preloading test, the water content is reduced to less than 45%. The interstitial water generated after flocculation can be extruded from the flocs by mechanical dewatering. The water content of the soil samples is lower than that of the control group after the vacuum preloading test.

Figure 10 shows the effect of different flocculants addition on the water content at depth of 0 cm, 20 cm, and 40 cm after the vacuum preloading. It is not difficult to find out that the water content of the control group is the highest at depth of 0 cm, 20 cm, and 40 cm, which is 43.19%, 46.58%, and 46.74%, respectively. The water content is 38.95% at the depth of 0 cm in the PAM, lower than that of other groups. At the depth of 20 cm, the lowest water content is 40.44% in the PAM+PSAF+lime. The lowest water content is 40.79% in the PAM+PSAF+lime when the depth is 40 cm.
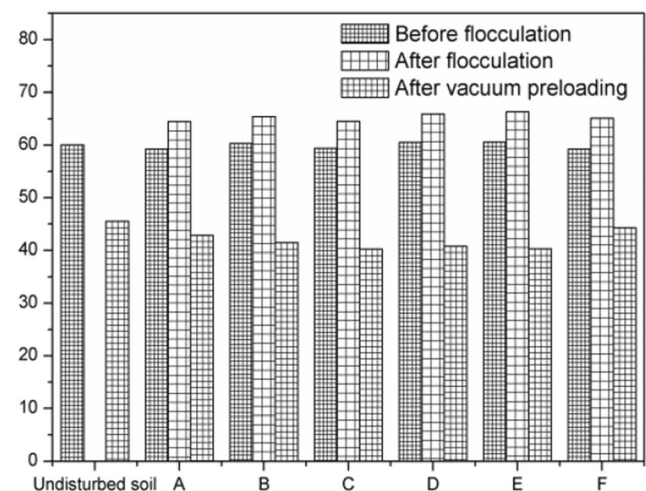


**Fig. 9** Water content before and after flocculation test and after vacuum preloading (PAM+PAC+lime (A), PAM+lime (B), PAM+PSAF+lime (C), PAM+PSAF (D), PAM (E), and PAM+PAC (F))
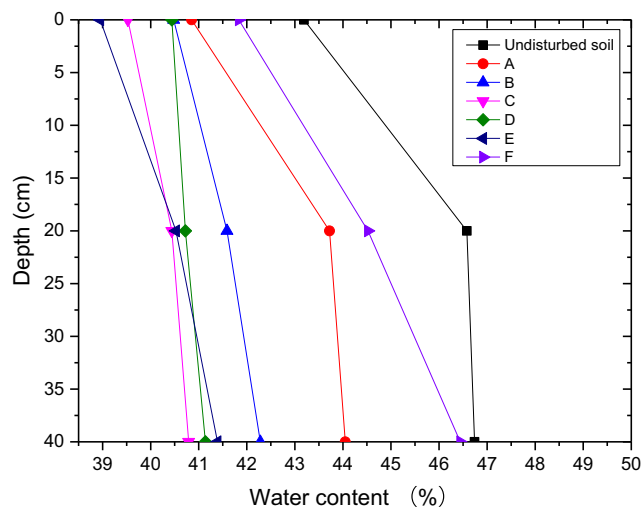
**Fig. 10** Water content of the soil samples at depth of 0 cm, 20 cm, and 40 cm after the vacuum preloading (PAM+PAC+lime (A), PAM+lime (B), PAM+PSAF+lime (C), PAM+PSAF (D), PAM (E), and PAM+PAC (F))

## Pore water pressure

In the vacuum preloading test, the pore water pressure detectors are located at depth of 20 cm and 40 cm in PAM+PAC+lime (A), PAM+lime (B), PAM+PSAF+lime (C), PAM+PSAF (D), PAM (E), and PAM+PAC (F). The depth of the control group is insufficient 40 cm in the same mass. Therefore, the pore water pressure at depth of 15 cm and 30 cm is measured in the control group. Figure 11 shows that the curves of pore water pressure at depth of 15 cm and 30 cm in the control group. The velocity of the pore water pressure decreases with increase of the depth, and the final dissipation value also decreases. The transmission of the vacuum degree can affect the pore water pressure and final dissipation value in the drainage board. The increase of
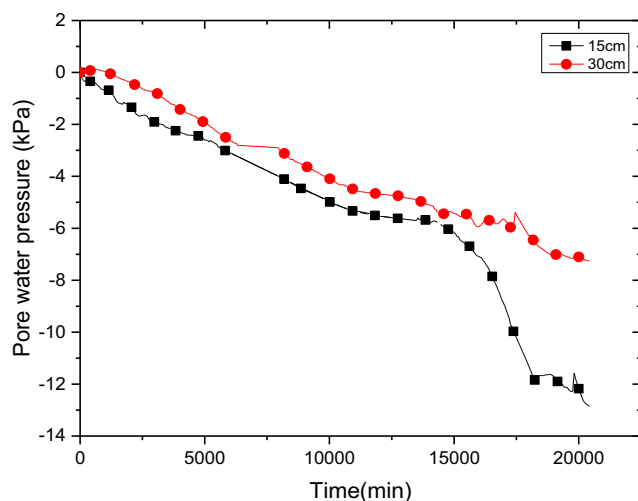


**Fig. 11** Curves of pore water pressure at depth of 15 cm and 30 cm in the control group (PAM+PAC+lime (A), PAM+lime (B), PAM+PSAF+lime (C), PAM+PSAF (D), PAM (E), and PAM+PAC (F))

depth and loss of the vacuum degree can also affect the consolidation of the lower soil.

Figure 12 shows that pore water pressure with time at depth of 20 cm and 40 cm, respectively. In general, the pore pressure dissipation of all the model barrels without the flocculating agents is the worst in terms of the dissipation rate and the final dissipation value. When the depth is at 20 cm, the final dissipated value of the PAM+PSAF+lime is the largest, reaching 16.867 kPa, which is 1.3 times higher than that of the control group. The fastest dissipating rate in the early stage is the PAM+PSAF. After 6000 min, the dissipating speed of the PAM+PSAF+lime is the fastest. When the depth is 40 cm, the PAM+PSAF+lime has the fastest dissipation rate and the final dissipation value, which indicates that the PSAF contributes to the dissipation of pore pressure. In the curves trend analysis, the pore water pressure of PAM+PAC+lime (A), PAM+lime (B), PAM+PSAF+lime (C), PAM+PSAF (D), PAM (E), and PAM+ PAC (F) do not reach a stable state at the same time, indicating that the incorporation of polyaluminium chloride do not significantly improve the pore dissipation rate and accelerate the drainage consolidation. The final dissipation value of pore water pressure in PAM+PAC+lime, PAM+lime, and PAM+ PSAF+lime is greater than that in PAM+PSAF, PAM, and PAM+PAC at depth of 20 cm and 40 cm. The incorporation of lime can increase the final dissipation value of pore water pressure. It can be found that the final dissipation value of the pore pressure in the PAM+PSAF+lime is higher than that of the PAM+lime, which is higher than that in the PAM+PAC+lime.

In summary, the addition of the flocculants contributes to the dissipation of pore pressure. The incorporation of the PSAF can accelerate the dissipation and increase the final dissipation value of pore water pressure. At the same time, the incorporation of lime under the same conditions can also increase the dissipation rate and final dissipation value of pore pressure. The effect of the incorporation of polyaluminium chloride on the dissipation rate of pore pressure is not significant.

## e-p curves

The upper and lower parts of the soil samples were tested by a ring cutter after vacuum preloading. The test instrument is equipped with a fully automatic air pressure consolidation instrument. The test load, the initial load, and the consolidation time are 8 grades, 12.5 kN, and 24 h, respectively. During the loading process, the test instrument can read the sedimentation amount of each stage in real time to obtain the following test data, as shown in Tables 4 and 5.

The value of the void ratio as a function of pressure can be calculated according to Eq. 2 (Liu et al. 2019; Dolinar and Trček 2019).

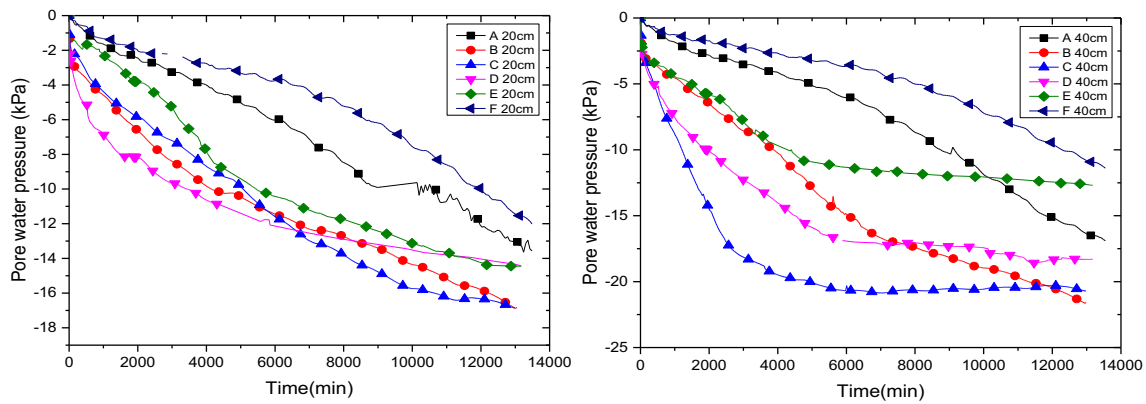$$e_i = e_0 - \frac{\Delta H_i}{H_0}(1+e_0) \qquad (2)$$

**Fig. 12** Pore water pressure curves at a depth of 20 cm and 40 cm (PAM+PAC+lime (A), PAM+lime (B), PAM+PSAF+lime (C), PAM+PSAF (D), PAM (E), and PAM+PAC (F))

where $e_0 = G_s(1 + w_0)(\rho_w/\rho_0) - 1$, $G_s$, $w_0$, $p_w$, and $p_0$ are the relative density of soil particles, the initial absolute moisture content of the soil samples, the density of water, and the initial density of the soil samples, respectively. The final result of the test is calculated according to Eq. 2, as shown in Fig. 13.

Figure 13 shows the results of the consolidation test of the control group, PAM+PAC+lime (A), PAM+lime (B), PAM+ PSAF+lime (C), PAM+PSAF (D), PAM (E), and PAM+PAC (F). It can be seen that the compression amount of the soil is substantially unchanged when the load is continuously loaded from 800 to 1600 kPa, indicating that the soil body is substantially in a compact state at this time in the control group. In the vacuum preloading, the consolidation effect on the upper and lower sides is relatively perfect, and the vacuum degree transmission is relatively uniform. The time of the consolidation test is 10 days. It can be obtained from Fig. 13 that the pore ratio is decrease when the previous load is between 0 and 200 kPa, and tends to be stable after 400 kPa. It is found that the stability of the lower soil samples is unchanged after each group reaching 800 kPa. The load of the upper soil samples is

continued to decrease after reaching 800 kPa. The upper soil samples cannot continue to upward transfer the vacuum degree due to the space limitation, so that the upper soil samples are not completely consolidated. The pore ratio will remain constant in the late pressurization.

In summary, the pore ratio decreases with the increase of the load and finally remains unchanged after reaching the stability. At the same time, the rate of change of the pore ratio becomes smaller as the load increases, indicating that as the pressure increases continuously, the soil particles gap is getting smaller and smaller. The compressibility of the soil is reduced until the change of void ratio is not obvious or remains unchanged.

## Compression modulus

The ratio of the decrease amount of the void ratio to the increase amount of the effective stress is the compression coefficient of the soil, that is, the secant slope of specific segment

**Table 4** Test results of upper side consolidation test

| Load/ kN | Compression amount/mm | | | | | | |
|---|---|---|---|---|---|---|---|
| | Blank | A1 | B1 | C1 | D1 | E1 | F1 |
| 12.5 | 1.258 | 0.412 | 0.332 | 0.166 | 0.34 | 0.468 | 0.116 |
| 25 | 1.794 | 0.732 | 0.666 | 0.46 | 0.742 | 0.858 | 0.467 |
| 50 | 2.624 | 1.421 | 1.328 | 0.888 | 1.265 | 1.668 | 1.154 |
| 100 | 3.678 | 2.699 | 2.44 | 1.582 | 2.223 | 2.912 | 1.56 |
| 200 | 4.864 | 4.071 | 3.845 | 2.443 | 4.038 | 4.321 | 2.07 |
| 400 | 6.133 | 5.322 | 5.125 | 3.535 | 4.086 | 4.381 | 3.389 |
| 800 | 7.204 | 6.41 | 6.252 | 6.541 | 6.517 | 6.93 | 4.628 |
| 1600 | 7.205 | 7.578 | 7.269 | 7.763 | 7.683 | 8.124 | 6.213 |

Note: A = PAM+PAC+lime; B = PAM+lime; C = PAM+PSAF+lime; D = PAM+PSAF; E = PAM; F = PAM+PAC

**Table 5** Test results of the lower side consolidation test

| Load/ kN | Compression amount/mm | | | | | | |
|---|---|---|---|---|---|---|---|
| | Blank | A2 | B2 | C2 | D2 | E2 | F2 |
| 12.5 | 1.143 | 0.816 | 0.597 | 0.49 | 0.437 | 0.379 | 1.137 |
| 25 | 3.086 | 1.502 | 0.976 | 0.91 | 0.733 | 0.792 | 2.09 |
| 50 | 4.256 | 2.558 | 1.522 | 1.306 | 1.191 | 1.615 | 3.336 |
| 100 | 5.346 | 3.784 | 2.797 | 2.619 | 2.482 | 2.871 | 4.561 |
| 200 | 6.432 | 5.134 | 4.416 | 4.185 | 4.176 | 4.303 | 5.782 |
| 400 | 7.444 | 6.409 | 5.774 | 5.535 | 4.256 | 4.357 | 6.907 |
| 800 | 7.762 | 7.375 | 5.775 | 6.663 | 6.906 | 6.797 | 7.847 |
| 1600 | 7.761 | 7.376 | 5.772 | 7.11 | 7.239 | 7.011 | 8.232 |

Note: A = PAM+PAC + lime; B = PAM+lime; C = PAM+PSAF+lime; D = PAM+PSAF; E = PAM; F = PAM+PAC

**Fig. 13** e-p curves of the control group, PAM+PAC+lime (A), PAM+lime (B), PAM+PSAF+ lime (C), PAM+PSAF (D), PAM (E), and PAM+PAC (F)
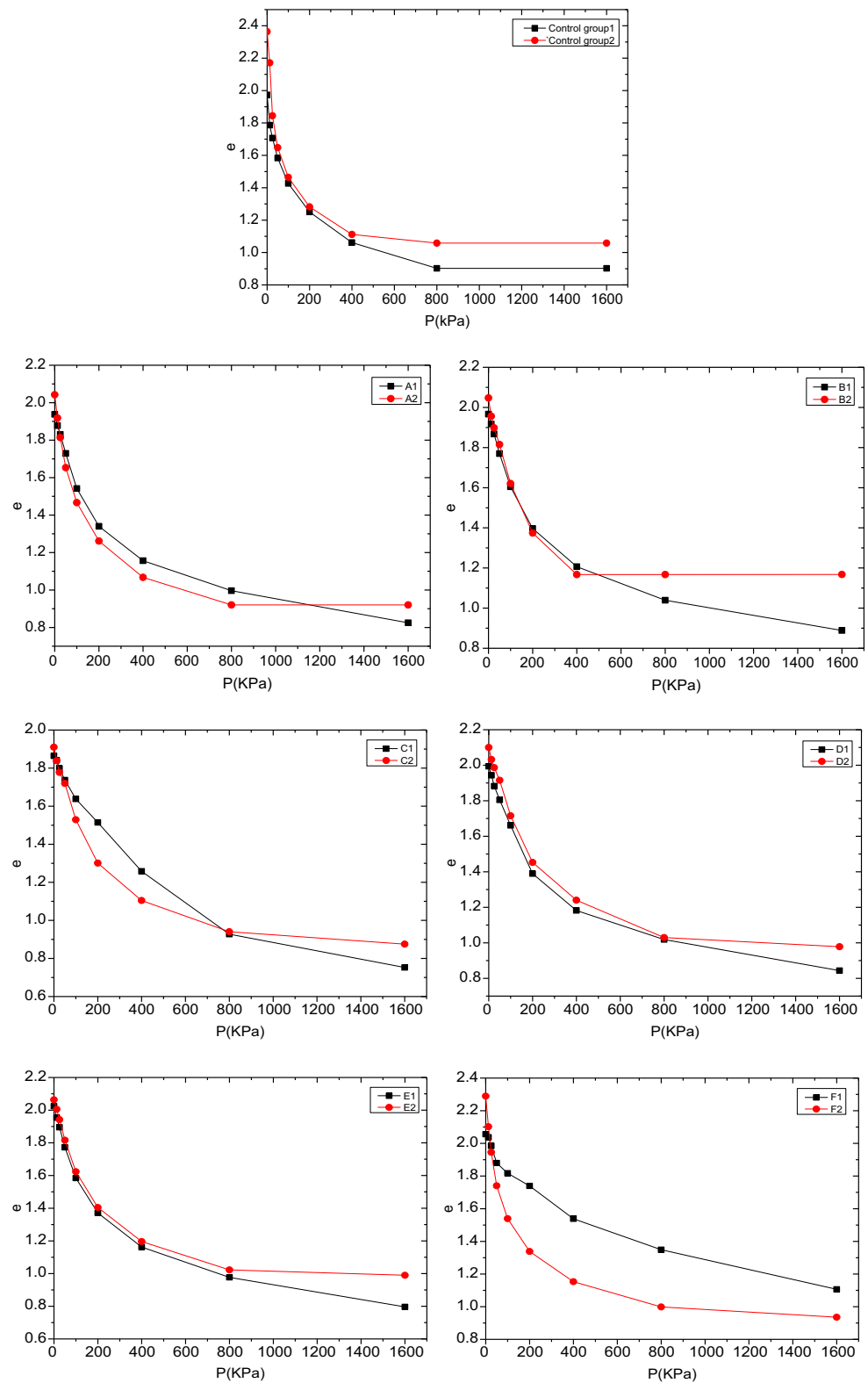


in the e-p curves. The compression coefficient of the soil can be calculated according to Eq. 3 (Fang et al. 2009b).

$$a = \frac{e_1 - e_2}{p_2 - p_1} \qquad (3)$$

where $a$ is the compression coefficient of the soil, MPa$^{-1}$; $P_1$ is the point "original pressure" in the soil, MPa; $P_2$ is the point "total pressure" in the soil, MPa; and $e_1$ and $e_2$ correspond to the pore ratio after

**Table 6** Calculation results of coefficient of consolidation $a_{1-2}$ and compression modulus

| No. | Absolute moisture content | Sample density | $ds$ | $e0$ | $H4$ | $H5$ | $e4$ | $e5$ | Compression coefficient $a_{1-2}$ (MPa$^{-1}$) | Compression modulus Es (MPa) | Compression modulus $E_{s,1-2}$ (MPa) |
|-----|------|------|-----|------|------|------|------|------|------|------|------|
| Blank | 0.7603 | 1.598 | 2.7 | 1.973 | 3.678 | 4.864 | 1.426 | 1.250 | 1.763 | 1.376 | 1.134 |
|  | 0.8252 | 1.465 | 2.7 | 2.363 | 5.346 | 6.432 | 1.464 | 1.281 | 1.826 | 1.349 | 1.095 |
| A | 0.6907 | 1.554 | 2.7 | 1.938 | 2.699 | 4.071 | 1.542 | 1.340 | 2.016 | 1.261 | 0.992 |
|  | 0.7873 | 1.586 | 2.7 | 2.042 | 3.784 | 5.134 | 1.467 | 1.261 | 2.054 | 1.201 | 0.974 |
| B | 0.6801 | 1.529 | 2.7 | 1.967 | 2.44 | 3.845 | 1.605 | 1.396 | 2.084 | 1.250 | 0.960 |
|  | 0.7326 | 1.535 | 2.7 | 2.047 | 2.797 | 4.416 | 1.621 | 1.374 | 2.467 | 1.063 | 0.811 |
| C | 0.6536 | 1.559 | 2.7 | 1.864 | 1.582 | 2.443 | 1.638 | 1.515 | 1.233 | 2.139 | 1.622 |
|  | 0.6790 | 1.558 | 2.7 | 1.910 | 2.619 | 4.185 | 1.529 | 1.301 | 2.278 | 1.110 | 0.878 |
| D | 0.6790 | 1.514 | 2.7 | 1.994 | 2.223 | 4.038 | 1.661 | 1.389 | 2.717 | 0.979 | 0.736 |
|  | 0.6989 | 1.480 | 2.7 | 2.100 | 2.482 | 4.176 | 1.715 | 1.453 | 2.626 | 1.034 | 0.762 |
| E | 0.6380 | 1.462 | 2.7 | 2.025 | 2.912 | 4.321 | 1.584 | 1.371 | 2.131 | 1.213 | 0.939 |
|  | 0.7062 | 1.504 | 2.7 | 2.064 | 2.871 | 4.303 | 1.624 | 1.405 | 2.194 | 1.196 | 0.912 |
| F | 0.7192 | 1.519 | 2.7 | 2.056 | 1.56 | 2.07 | 1.818 | 1.740 | 0.779 | 3.616 | 2.567 |
|  | 0.8672 | 1.533 | 2.7 | 2.289 | 4.561 | 5.782 | 1.539 | 1.338 | 2.008 | 1.264 | 0.996 |

Note: A = PAM+PAC+lime; B = PAM+lime; C = PAM+PSAF+lime; D = PAM+PSAF; E = PAM; F = PAM+PAC

compression and stabilization under the action of $P_1$ and $P_2$.

In order to facilitate the comparison of the data, the compressibility of the soil is generally evaluated by increasing the compression coefficient $a_{1-2}$ when $p_1$ (0.1 MPa) is increased to $p_2$ (0.2 MPa).

Wherein, when $a_{1-2} < 0.1$ MPa$^{-1}$, it is a low compressibility soil;

When $0.1 \leq$ MPa$^{-1} a_{1-2} < 0.5$ MPa$^{-1}$, it is medium compressive soil;

When $a_{1-2} \geq 0.5$ MPa$^{-1}$, it is a high compressibility soil.

The compression modulus of the soil represents the ratio of the vertical additional stress to the strain during the stressing of the soil process, can be calculated according to Eq. 4 (Fang et al. 2009b).

$$E_S = \frac{1 + e_1}{a} \tag{4}$$

where $Es$ is expressed as the compression modulus of the soil (MPa), $a$ is the compression coefficient of the soil (MPa$^{-1}$), and $e_1$ is the void ratio corresponding to compression stability under the action of $P_1$.

The coefficient of consolidation ($a_{1-2}$) and compression modulus of the control group, PAM+PAC+lime (A), PAM+lime (B), PAM+PSAF+lime (C), PAM+PSAF (D), PAM (E), and PAM+PAC (F) can be calculated according to Eqs. 3 and 4, respectively. The calculation results are shown in Table 6.

It can be seen that coefficient of consolidation ($a_{1-2}$) is bigger than 0.5 MPa$^{-1}$, and the compression modulus ($E_{s,1-2}$) is lower than 4 MPa, as shown in Table 6. The soil samples

are all high compressibility soil after vacuum preloading. The compression modulus increases gradually and the coefficient of consolidation decreases gradually with the increase of the external load. At the same time, the larger the coefficient of consolidation, the higher for the compressibility of the soil. The compression modulus is smaller when the compressibility is higher in the soil. It can be found that the compressibility of the upper soil is lower than that of the lower soil (Table 6). The compressibility of the PAM+PSAF is the highest. The compressibility of the upper and lower soil of PAM+PSAF+lime and PAM+PAC is larger than other groups. The control group has the lowest compressibility. The addition of lime has little effect on the compressibility of the soil samples after the
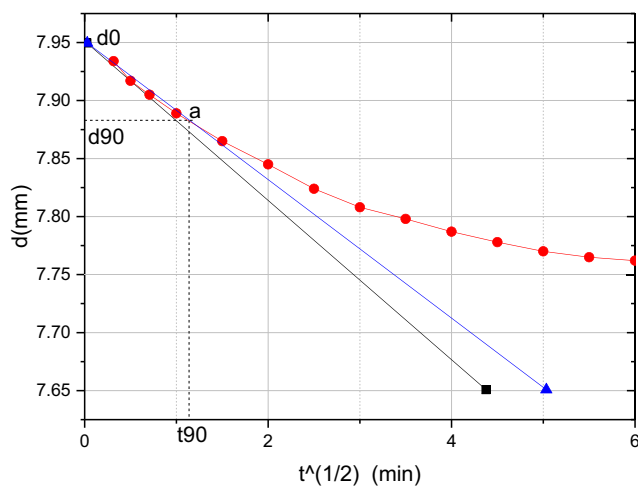


**Fig. 14** Calculation method of the coefficient of consolidation

**Table 7** Calculation results of coefficient of consolidation

| Load P(kPa) | Blank | A | B | C | D | E | F |
|---|---|---|---|---|---|---|---|
| 12.5 | 0.0081 | 0.4669 | 0.23713 | 0.11043 | 0.08963 | 0.08518 | 0.76832 |
| 25 | 0.0174 | 0.24491 | 0.12652 | 0.06997 | 0.08751 | 0.15618 | 0.22207 |
| 50 | 0.0122 | 0.05588 | 0.04947 | 0.06682 | 0.06436 | 0.05619 | 0.15398 |
| 100 | 0.01709 | 0.12334 | 0.0555 | 0.05961 | 0.04915 | 0.03246 | 0.29752 |
| 200 | 0.01855 | 0.03574 | 0.03171 | 0.05662 | 0.02924 | 0.02697 | 0.23966 |
| 400 | 0.02871 | 0.02163 | 0.02687 | 0.05225 | 0.02922 | 0.02132 | 0.07533 |
| 800 | 0.04577 | 0.05696 | 0.05196 | 0.00557 | 0.02341 | 0.0203 | 0.12421 |
| 1600 | – | 0.05712 | 0.06697 | 0.05299 | 0.08352 | 0.06681 | 0.0879 |

Note: A = PAM+PAC+lime; B = PAM+lime; C = PAM+PSAF+lime; D = PAM+PSAF; E = PAM; F = PAM+PAC

vacuum preloading in PAM+PAC+lime and PAM+PAC, PAM+lime and PAM, PAM+PSAF+lime, and PAM+PSAF. Therefore, the addition of the flocculants can improve the compressibility, increase the pore ratio, expand the water passage, and accelerate the discharge of water.
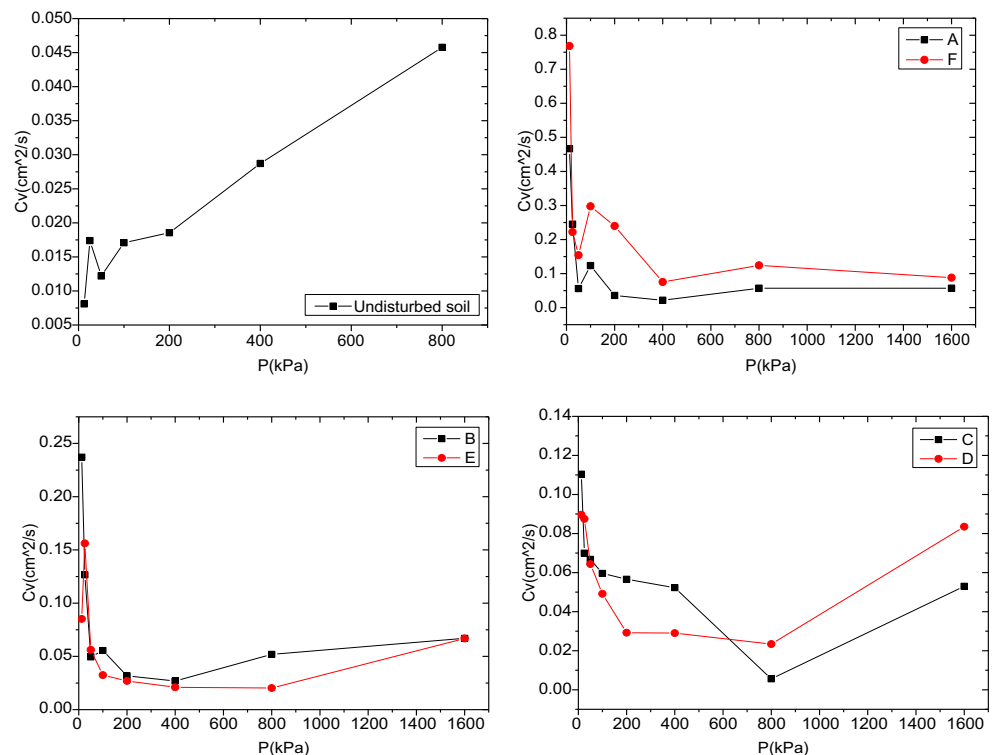
## Coefficient of consolidation

The coefficient of consolidation for the soil reflects the speed of soil consolidation. The coefficient of consolidation is larger when the discharge of the pore water is faster in the soil. The readings of the dial gauge, the time recorded, and the coefficient of consolidation are calculated by the square-root-of-time rule in the consolidation test. Firstly, the reading data of

dial indicators obtained by the consolidation test is plotted on the ordinate, and the square root of the time $(d-\sqrt{t})$ is plotted on the abscissa. The beginning of the extended curve $(d-\sqrt{t})$ is obtained as a straight line segment, intersecting the ordinate with a point $ds$, passing $ds$ and the abscissa is 1.15 times of the front line segment. The curve $(d-\sqrt{t})$ intersects with the point a, coordinates are $(t_{90}, d_{90})$, and $t_{90}$ represents the time required for the soil samples to have a consolidation degree of 90%, as shown in Fig. 14.

The coefficient of consolidation can be calculated according to Eq. 5 (Olek 2019):

$$C_v = \frac{0.848h^2}{t_{90}} \tag{5}$$

**Fig. 15** Coefficient of consolidation of the control group, PAM+PAC+lime (A), PAM+lime (B), PAM+PSAF+lime (C), PAM+PSAF (D), PAM (E), and PAM+PAC (F)

where $C_v$ is the coefficient of consolidation, cm$^2$/s; $h$ represents the maximum drainage distance equal to a half of the average value of the initial and end heights of the samples at a certain level of pressure, cm; and $t_{90}$ is the time required for the consolidation degree reached 90%, s.

According to the above Eq. 5, the coefficient of consolidation for the control group, PAM+PAC+lime (A), PAM+lime (B), PAM+PSAF+lime (C), PAM+PSAF (D), PAM (E), and PAM+PAC (F), is calculated, and the calculation results are shown in Table 7.

The coefficient of consolidation for each group was plotted under different loads (12.5–800 kPa), as shown in Fig. 15. The coefficient of consolidation increases with the increase of pressure in the control group. The consolidation state remains constant when the load reaches 800 kPa. However, the trend of decreasing firstly and then increasing (excluding the increasing section starting from 0) is observed for PAM+PAC+lime (A), PAM+lime (B), PAM+PSAF+lime (C), PAM+PSAF (D), PAM (E), and PAM+PAC (F). When the consolidation load starts from 0, the coefficient of consolidation will reach maximum, and then begins to decline. This may be because the structure of the initial soil is not completely destroyed, and the drainage resistance is large in the soil, which affects the increase of the coefficient of consolidation. In addition, the coefficient of consolidation of each group is greater than the control group. Therefore, the overall effect of the PAM is optimal according to the flocculants price, dewatering effect, water quality, vane shear strength, compression coefficient, and coefficient of consolidation after flocculation-vacuum preloading in the treatment of the river sediments.

## Conclusions

In the flocculation-vacuum preloading test, the moisture content of the soil samples could be increased to about 65% after flocculation, and the soil state was changed from plastic flow to plastic state. After the vacuum preloading test, the moisture content of the soil samples decreased to less than 45%, and the lowest reached 40.25%. At the same time, the lowest water content was 38.95% when the depth was 0 cm in the PAM. The PAM had the best effect in the vane shear strength test. The price of the PAM is lower than dual and tertiary treatments. The PAM+PSAF had the fastest water discharge rate and the largest displacement during the vacuum preloading test, which was 187% of the control group. In PAM+PSAF, the incorporation of lime not only reduced the drainage rate but also reduced the final displacement. However, the overall effect of the PAM is optimal.

## References

Akcay H, Oguz A, Karapire C (2003) Study of heavy metal pollution and speciation in Buyak Menderes and Gediz river sediments. Water Res 37:813–822

Chai J, Rondonuwu SG (2015) Surcharge loading rate for minimizing lateral displacement of PVD improved deposit with vacuum pressure. Geotext Geomembr 43:558–566

Dolinar B, Trček B (2019) A new relationship between the mobile and the adsorbed water in fine-grained soils using an effective void-ratio estimation. B Eng Geol Environ 78:4623–4631

Emelyanov EM, Kravtsov VA (2007) Cause of elevated as concentrations in the Baltic Sea and Vistula lagoon. Geochem Int 45:798–815

Fang YG, Guo LF, Huang JW (2019a) Mechanism test on inhomogeneity of dredged fill during vacuum preloading consolidation. Mar Georesour Geotec 37:1007–1017

Fang XH, Peng B, Wang X, Song ZL, Zhou DX, Wang Q, Qin ZL, Tan CY (2019b) Distribution, contamination and source identification of heavy metals in bed sediments from the lower reaches of the Xiangjiang River in Hunan province. China Sci Total Environ 689:557–570

Huang R, Liu J, Wang ZF, Gao M (2019) Effects of different soil amendments application on soil aggregate stability and soil consistency. Commun Soil Sci Plan 50:2263–2277. https://doi.org/10.1080/00103624.2019.1659296

Jankowski KL, Törnqvist TE, Fernandes AM (2017) Vulnerability of Louisiana's coastal wetlands to present-day rates of relative sea-level rise. Nat Commun 8:14792

Jin QB, Li YB, Li B (2019) Consolidation behavior and elastic wave characteristics of lime-treated dredged mud with vacuum preloading. Mar Georesour Geotec:1–10. https://doi.org/10.1080/1064119X.2019.1679927

Kjellman W, 1952 Consolidation of clay soils by atmospheric pressure. In: Proc. Conf. Soil Stab. Massach. Inst. Technol, Boston, pp. 258–263

Lafhaj Z, Samara M, Agostini F, Boucard L, Skoczylas F, Depelsenaire G (2008) Polluted river sediments from the North region of France: treatment with Novosol (R) process and valorization in clay bricks. Constr Build Mater 22:755–762

Liu GP, Cai SQ (2019) Modeling of suspended sediment by coupled wave-current model in the Zhujiang (Pearl) River Estuary. Acta Oceanol Sin 38:22–35

Liu MW, Wang CZ, Bai Y, Xu GR (2018) Effects of sintering temperature on the characteristics of lightweight aggregate made from sewage sludge and river sediment. J Alloy Compd 748:522–527

Liu ZR, Ye WM, Zhang Z, Wang Q, Chen YG (2019) A nonlinear particle packing model for multi-sized granular soils. Constr Build Mater 221:274–282

Olek BS (2019) Critical reappraisal of Casagrande and Taylor methods for coefficient of consolidation. KSCE J Civ Eng 23:3818–3830

Pejman A, Nabi Bidhendi G, Ardestani M, Saeedi M, Baghvand A (2015) A new index for assessing heavy metals contamination in sediments: a case study. Ecol Indic 58:365–373

Samara M, Lafhaj Z, Chapiseau C (2009) Valorization of stabilized river sediments in fired clay bricks: factory scale experiment. J Hazard Mater 163:701–710

Sun L, Gao X, Zhuang D, Guo W, Hou J, Liu X (2018) Pilot tests on vacuum preloading method combined with short and long PVDs. Geotext Geomembr 46:243–250

Teatini P, Tosi L, Strozzi T (2011) Quantitative evidence that compaction of Holocene sediments drives the present land subsidence of the Po Delta, Italy. JGeophys Res Solid Earth 116(B8)

Trojanowska M, Świetlik R (2019) The importance of drying and grinding samples for determining mobile chromium fractions in polluted river sediments. Environ Monit Assess 191:578

Wang P, Han YB, Wang J, Cai YQ, Geng XY (2019) Deformation characteristics of soil between prefabricated vertical drains under vacuum preloading. Geotext Geomembr 47:798–802

Wang J, Gao ZY, Fu HT, Ding GY, Cai YQ, Geng XY, Shi CX (2019a) Effect of surcharge loading rate and mobilized load ratio on the performance of vacuum–surcharge preloading with PVDs. Geotext Geomembr 47:121–127

Wang J, Huang G, Fu HT, Cai YQ, Hu XQ, Lou XM, Jin JW, Hai J, Ni JF, Zou J (2019b) Vacuum preloading combined with multiple-flocculant treatment for dredged fill improvement. Eng Geol 259: 105194

Xia P, Meng XW, Feng AP, Yin P, Wang XQ, Zhang J (2012) Pb-210 chronology and trace metal geochemistry in the intertidal sediment of Qinjiang River estuary. China J Ocean U China 11:165–173

Zhu WL, Cui LH, Ouyang Y, Long CF, Tang XD (2011) Kinetic adsorption of ammonium nitrogen by substrate materials for constructed wetlands. Pedosphere 21:454–463

Zhu GF, Shi PJ, Pu T, He YQ, Zhang T, Wang PZ, Pan MH (2013) Changes of surface soil relative moisture content in Hengduan Mountains, China, during 1992-2010. Quatern Int 298:161–170